Energy 307 (2024) 132793

Contents lists available at ScienceDirect

Energy

journal homepage: www.elsevier.com/locate/energy

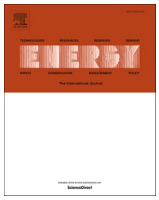

# Numerical and experimental investigation of a single-body PVT using a variable air volume control algorithm

Ahmet Aktaş [a], Meltem Koşan [b], Burak Aktekeli [c,d], Yaren Güven [a,*], Erhan Arslan [e], Mustafa Aktaş [a]

[a] Gazi University, Faculty of Technology, Energy Systems Engineering, Turkey
[b] Kahramanmaraş İstiklal University, Elbistan Faculty of Engineering, Energy Systems Engineering, Turkey
[c] Gazi University, Natural and Applied Science Institute, Turkey
[d] Bilecik Şeyh Edebali University, Osmaneli Vocational School, Worker Health and Safety, Turkey
[e] TÜBİTAK Marmara Research Center, Turkey

ARTICLE INFO

Handling editor: X Zhang

*Keywords:*
Solar energy
PVT
Temperature control
Eco-design
Variable air volume

ABSTRACT

Photovoltaic thermal (PVT) collectors that can achieve maximum efficiency from solar irradiation can be critical concepts for meeting energy demand in residential applications. Even though there is much research on increasing heat transfer, multifunctional designs that provide homogeneous results are limited. This study explores the production of electricity and hot air from a novel design of a PVT. A new perforated copper plate design has been proposed to achieve maximum efficiency by providing homogeneous cooling in the PVT. Firstly, numerical analysis of this design was performed using Ansys Fluent software, then tested experimentally. The highest and average electrical and thermal efficiency of PVT are obtained as 17.62 %, 15.63 %, and 76.75 %, 43.68 %. In experiments conducted under winter conditions, the maximum temperature value in the PVT was measured as 41.54 °C. Moreover, the payback period of the PVT system was calculated as 6.1 years. The proposed PVT collector can be used as a new model for integrating solar energy in buildings with almost zero energy. Considering the eco-design, this PVT design can contribute net positive carbon, ecological footprint, and green manufacturing.

## 1. Introduction

With the advancement of technology and the dynamic rise in population, energy consumption is also expanding rapidly. Recently, there has been an effort to use sustainable and renewable energy to reduce the carbon emissions associated with electric and thermal energy demand [1,2]. Solar energy is the best clean, sustainable, inexhaustible energy to meet these efforts. Among solar energy technologies, photovoltaic thermals (PVT) are the most established green technologies worldwide. Since PVTs can generate electrical and thermal energy, they are an excellent alternative to meet energy needs, especially in building applications. Additionally, PVTs are advantageous regarding capital investment, commercial expansion, affordability, and compactness [3–5].

It is aimed to increase the efficiency of the photovoltaic (PV) collector by cooling and obtaining thermal energy by absorbing the heat from the PV surface. PV collectors are cooled with working fluids such as air [6–8], water [9,10], refrigerant [11,12], nanofluid [13,14], etc., and heat energy is withdrawn from the surface. In this way, thermal energy is provided by solar irradiation in addition to electrical energy. In addition, heat transfer performance can be enhanced by employing ribs, fins, or inserts. Fins provide temperature consistency, increase convective heat transfer, enhance heat dissipation, improve thermal absorption, and improve overall PVT system performance and efficiency. Air is beneficial for heat transmission and storage in PVT systems because of its high specific heat capacity, which makes it possible for thermal energy to be absorbed and stored efficiently per unit mass [15,16].

In their study, Arslan et al. [17] developed and evaluated a novel air-cooled monocrystalline photovoltaic tube, including air-fluidized glass glass and copper fins. The system's efficiency was calculated before the experiments using computational fluid dynamics (CFD) research. This study's researchers conducted computational and experimental analyses of various mass flow rates. In conclusion, they observed that the PV surface temperature decreased as the mass flow rate increased while the efficiency increased by 0.42 %. When the flow rate was 0.031087 kg/s, the thermal efficiency of PVT was 37.10 %, and the

* Corresponding author.
*E-mail address:* yarenguven@gazi.edu.tr (Y. Güven).

https://doi.org/10.1016/j.energy.2024.132793
Received 15 April 2024; Received in revised form 19 July 2024; Accepted 8 August 2024
Available online 10 August 2024

**Nomenclature**

*Acronyms*

| | |
|---|---|
| CFD | computational fluid dynamics |
| COP | coefficient of performance |
| DC | direct current |
| MPP | maximum power point |
| NTC | negative temperature coefficient |
| PV | photovoltaic |
| PVT | photovoltaic thermal collector |
| SD | secure digital |

*Symbols*

| | |
|---|---|
| $A$ | area ($m^2$) |
| $A_c$ | collector area ($m^2$) |
| $AC$ | annual amount ($/year) |
| $c_p$ | specific heat capacity (J/kgK) |
| $\dot{E}_x$ | exergy (W) |
| $ET$ | unit price of electricity ($/kWh) |
| $I$ | current (A) |
| $\dot{m}$ | mass flow rate of air (kg/s) |
| $M_{gas}$ | amount of natural gas ($m^3$) |
| $N$ | daily working time in a year (h) |
| $P$ | power (W) |
| $PP$ | payback period (year) |
| $NT$ | unit price of natural gas ($/$m^3$) |
| $R$ | measured quantity |
| $S$ | solar irradiation ($W/m^2$) |
| $\dot{Q}$ | thermal power (W) |
| $\dot{Q}_u$ | useful energy (W) |
| $T$ | temperature (K) |
| $TIC$ | total investment cost ($) |
| $V$ | voltage (V) |
| $W_R$ | total uncertainty |

*Greek*

| | |
|---|---|
| $\rho$ | density ($kg.m^3$) |
| $\eta$ | efficiency (%) |
| $\nu$ | velocity (m/s) |

*Subscripts*

| | |
|---|---|
| $a$ | ambient |
| $d$ | destruction |
| $el$ | electric |
| $ex$ | exergy |
| $irr$ | irradiation |
| $in$ | inlet |
| $max$ | maximum |
| $s$ | sun |
| $out$ | outlet |
| $th$ | thermal |
| $x$ | independent variables |
| $w$ | error rates |

electrical efficiency was 13.56 %. The thermal efficiency and electrical efficiency of PVT were obtained as 49.5 % and 13.98 % when the flow rate was 0.04553 kg/s. Abuşka and Şevik [18] experimentally investigated aluminum flat-plate solar collectors, copper flat-plate solar collectors, v-groove aluminum solar collectors, and v-groove copper solar collectors at different mass flow rates. Mass flow rates were taken as 0.04 kg/s, 0.06 kg/s, 0.08 kg/s, and 0.1 kg/s in the experiments. They found that the thermal and exergy efficiencies of the collectors were 43–60 % and 6 − 12 %, respectively. The average payback value was found to be 4.3 − 4.6 years. The collector with the highest thermal performance was the copper v-groove collector. Yu et al. [19] made a PVT with a single piece of glass cover and an interior chamber that kept the top and bottom of the absorber in a vacuum state. They then tested it against an air-gap PVT to see which worked better. At 50 °C, the vacuum plate PVT had much better temperature performance than the air-gap PVT. When there is no air in the room, the heat loss index drops by 16.08 %. This could increase the rate at which solar energy is utilized by making the system process longer in the winter. In their study, Guo et al. [20] examined a PVT that possessed a tri-functional design. Water was used as a working fluid. The researchers got yearly thermal efficiencies of 38.5 %, 38.9 %, and 40.1 % for the PVT conducted in Hefei, Beijing, and Xining. They concluded that the tripartite PVT exhibited higher efficiency than the individual PVT water and air collectors. Kumar and Rosen [21] examined the performance of their proposed PVT in two cases, with and without fins. It was observed that when the absorber area was expanded in the finned system, heat transfer increased, and the cell temperature decreased. With the addition of the fins, thermal and electrical efficiency increased to 15.5 % and 10.5 % respectively. Maurya et al. [22] designed a tubular three-pass solar air heater and tested it at different air mass flow rates under glazed and unglazed conditions. Three passes, five tubes per pass for 15 tubes, were placed close to each other. The thermal efficiency of the three-pass solar air heater increased with increasing air flow rate. At 0.006 kg/s, 0.004 kg/s, and 0.002 kg/s air flow rates, the maximum thermal efficiency was 60.04 %, 41 %, and 33.3 %, respectively. Higher thermal efficiency was achieved in the glazed case than in the unglazed case. The maximum value of the outlet air temperature for the three-pass solar air heater was 110.6 °C at an airflow rate of 0.002 kg/s.

Joo et al. [23] experimentally examined three different PVT modules: a glazed PVT module with a transparent film, a glazed PVT module with glass, and an unglazed PVT module with glass. The glazed PVT module with a transparent film achieved maximum efficiency of approximately 71.1 %. Additionally, it was observed that 8187.1 kWh of heat and 4430.1 kWh of electricity could be obtained with the PVT system integrated into the roof. Hamada et al. [24] analyzed the performance of a photovoltaic thermal system with three different water-based absorber designs. In the proposed system, the maximum total efficiency was 69.6 % at a water flow rate of 3 L/min. Emam et al. [25] investigated an innovative water-based PVT system combined with phase change material. As a result, a decline in PVT cell temperature of up to 8.3 °C, an enhancement in electrical efficiency of up to 13.3 %, and an increase in power output of up to 15.9 %. Zareie et al. [26] numerically examined 15 different roll bond designs in the PVT system. The optimum electrical and thermal efficiency of PVT was 17.75 % and 61.86 %. Arslan et al. [27] numerically and experimentally studied new air-cooled PVT with copper fins with variable airflow. The average thermal, electrical, and exergy efficiency of PVT were obtained as 32.71 %, 12.77 %, and 12.97 %. It was concluded that as the voltage of the fan increased, the thermal and electrical performance was also enhanced. Khelifa et al. [28] numerically investigated the cooling of a PVT collector consisting of fins attached to aluminum tubes with both water and air. It was observed that thermal and electrical performance improved as the number of fins increased from 20 to 40 in this bifluid system. The best thermal efficiency was achieved as 54.25 % at a water flow rate of 0.01 kg/s and a design with 40 fins.

Based on this brief literature review, even though some research has been conducted on air-based PVTs, there still needs to be more compact design, high efficiency, and applicability in buildings. Therefore, in this study, a newly compact design is described and evaluated to enable the production of heat and electricity for buildings. The following


**Fig. 1.** Structure of the main steps of the study.

contributions are performed in this article.

- A new air-based PVT design with a perforated copper plate is proposed.
- A new temperature control with a variable air volume collector has been designed to adjust the flow rate of the fans depending on the back surface temperature of the PV.
- A numerical model is developed and validated to examine how to be homogeneously in the PVT's airflow.
- The experimental analysis of the PVT is conducted using numerical analysis.

The variable air volume control recommended in the study constantly changes the fan speed according to the collector surface temperature. This developed control algorithm aims to cool the PV collector with lower fan power. Thus, less energy is consumed in cooling the PV collector than fan systems that cool with constant speed and power. The current research with a new design offers it to maximize energy utilization efficiency and reduce thermal losses in PVTs. Fig. 1 indicates the main steps of this study. Firstly, a numerical analysis of the proposed PVT system was carried out. Then, it was manufactured and tested experimentally. Detailed information about numerical analysis and experimental studies was given in the Material and Methods section. The Results and Discussion section discussed the obtained numerical and experimental findings. Finally, the results of the study are summarized in the Conclusion.

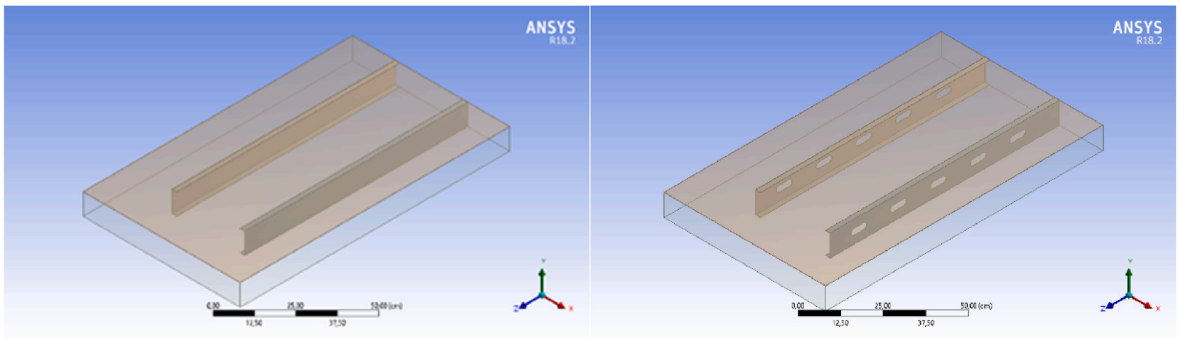


**Fig. 2.** Representation of geometry: a) non-perforated collector geometry and b) perforated collector geometry.

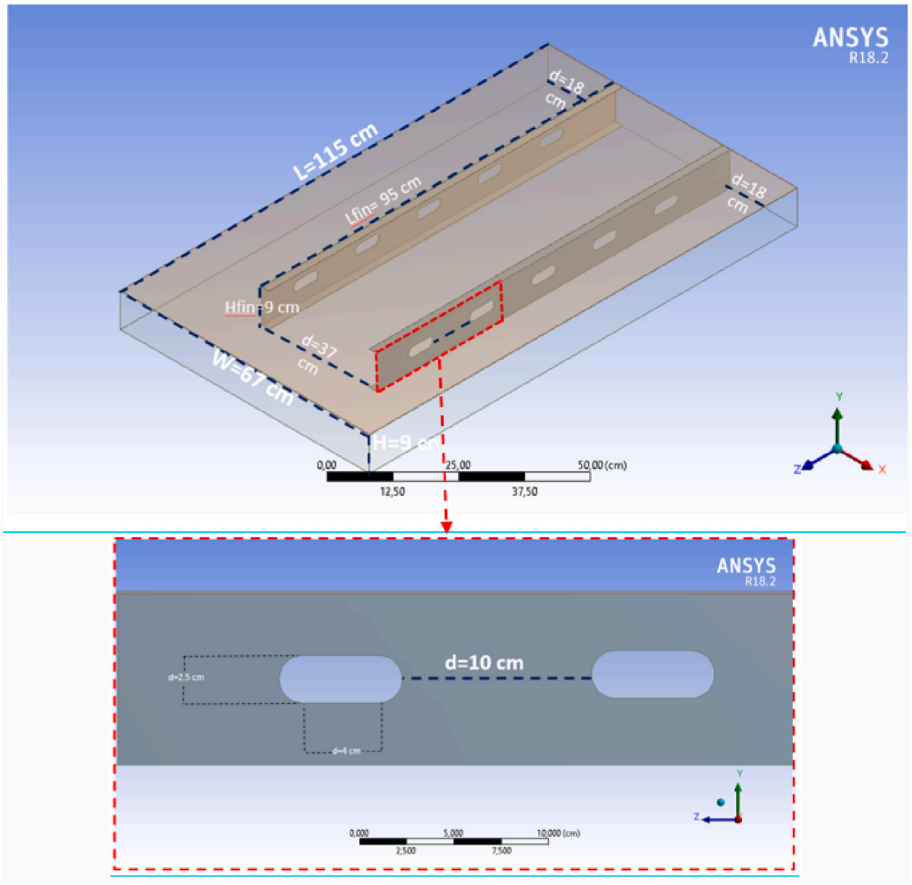


**Fig. 3.** Measurement of collector and fin structure.

## 2. Material&Methods

In this study, two different designs were made with two copper plates behind the PVT. These copper plates are designed to be perforated and non-perforated. First, a numerical analysis of these designs was carried out to observe the speed and temperature distributions of the air entering the collector. Then, the experimental setup was manufactured according to the results of the numerical analysis. The proposed PVT was performed experimentally for three days.

### *2.1. Numerical analysis*

#### *2.1.1. Creation of geometric structure*

This study employed numerical analysis to investigate airflow analysis in photovoltaic/thermal systems. The numerical analysis was conducted using the Ansys program. The CFX module, comprising numerous sub-modules dedicated to computational fluid dynamics, exhibits several advantages over alternative modules. These advantages encompass a user-friendly interface, domain determination capabilities, and accommodating diverse turbulence models. The CFX module was chosen as the preferred method for conducting numerical analysis in this studydue to its numerous advantages. The geometry of the collector was created using the "Design Modeler" program, a subprogram of the Ansys

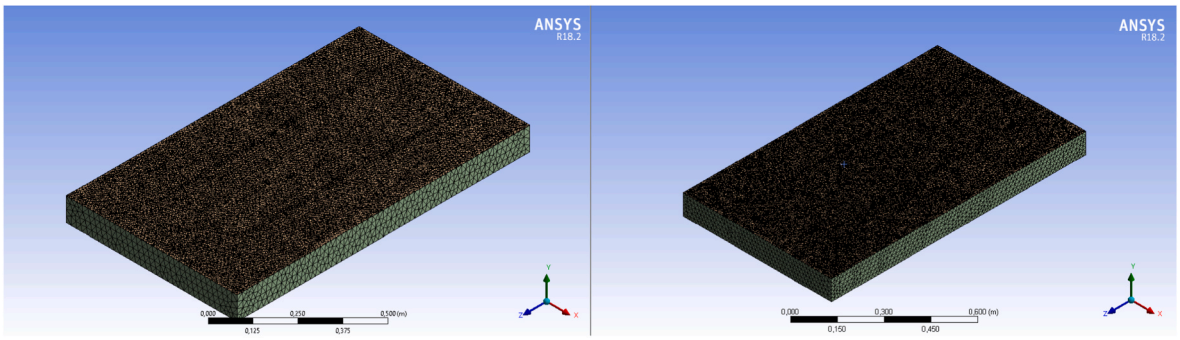


**Fig. 4.** The mesh structure of the geometry: a) non-perforated, b) perforated.

**Table 1**
Thermophysical features are required for numerical analysis.

| Parameters | $c_p$ (J/kgK) | $\rho$ (kg/m$^3$) | $k$ (W/mK) | $\delta$ (mm) |
|---|---|---|---|---|
| Air | 1004.4 | 1.19 | 0.0261 | 125 |
| PV Module | 668 | 2331 | 148 | 0.15 |
| Cooper Fins | 385 | 8933 | 401 | 1 |
| Insulation | 880 | 15 | 0.041 | 50 |

program. The structure of the collector is depicted in Fig. 3.

### 2.1.2. Fin structure

The numerical analysis considered two distinct scenarios (Fig. 3). In the initial scenario (Fig. 2a), the outcomes were acquired in the absence of copper fin drilling, while in the subsequent scenario, the outcomes were obtained through fin drilling. In the second scenario, five elliptical apertures, measuring 2.5 cm in width, 4 cm in length, and spaced 10 m apart, were perforated into the copper fins (Fig. 2b).

### 2.1.3. Mesh structure

Mesh structure creation refers to partitioning a geometric structure based on the number of elements and nodes present. According to Ref. [29], a positive correlation exists between the number of elements or nodes and the accuracy of the results. Utilizing mesh elements of smaller sizes close to the wall yields favorable resolution in capturing the boundary layer and temperature field gradients. This holds particular significance for inflows encompassing a natural convection boundary layer. The mesh structure of the system is depicted in Fig. 4. Upon completion of the construction, the suitability center determined that "Fine" was the preferred option, while "medium" was chosen to mitigate the size.

### 2.1.4. Initial and boundary conditions

In all experiments, the temperature of the air entering the collector was chosen as 25 °C based on numerical analysis. A solar irradiation value of 565 W/m$^2$ was selected for the collector surface, representing Ankara's annual average irradiation value. The source of this value is Türkiye Global Irradiation Values [30]. Table 1 presents the thermophysical properties necessary for numerical analysis, with the fins being selected as copper material. The collector's sides were selected as adiabatic walls. The PV module surface was designated as the "heat flux" surface, while the remaining surfaces were designated as "wall" surfaces and selected using adiabatic methods. A "no slip condition" was implemented on all walls. The uniform application of the mass flow rate was observed in the inlet area. Zero is introduced as the average static pressure in the outlet section.

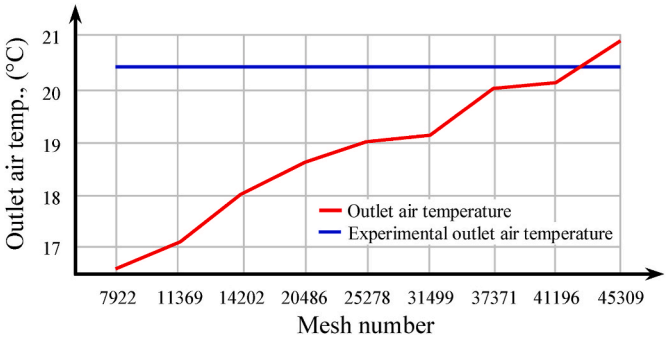


**Fig. 5.** Mesh independence test.

### 2.1.5. The procedure of Ansys solution

The numerical study was conducted with initial and boundary conditions to ensure that the air inlet and ambient air temperatures were equal. The pressure at the edges before opening is measured to be 101325 Pa. The working fluid is air, the collection is thought of in three dimensions, and steady-state conditions are used. The solar irradiation stays the same, and the flow is rough. The convergence of the velocity components for their "residuals" is taken as 10E-6 in the continuity equation. A finite volume algorithm and a second-order upwind scheme were chosen to solve the main equations (continuity, momentum, energy). The SIMPLE algorithm was chosen to discretize the governing equations. The main equations, including fluid continuity (Eq. (1)), momentum (Eqs. (2) and (3)), and energy (Eq. (4)) equations, were chosen to test the suitability and applicability of the model regarding their motion.

Continuity equation:

$$\partial\rho / \partial t + \nabla(\rho v) = 0 \tag{1}$$

Momentum equations:

$$(\partial(\rho u)) / \partial t + \nabla(\rho u V) = -\partial p/\partial x + \mu\nabla(\nabla u) + \rho g_x \tag{2}$$

$$(\partial(\rho v)) \Big/ \partial t + \nabla(\rho v V) = -\partial p \Big/ \partial x + \mu\nabla(\nabla v) + \rho g_y \tag{3}$$

Energy equation:

$$\left(\rho c_p (dT / dt + \nabla T V)\right) = \nabla(\nabla k T) \tag{4}$$

### 2.1.6. Mesh independence test

To conduct numerical analysis in the study, it is necessary to ascertain the optimal mesh number. In the present study, the analysis of mesh numbers 7922 – 45309 led to the identification of the optimal mesh number as 45309. Numerical and experimental results of outlet air

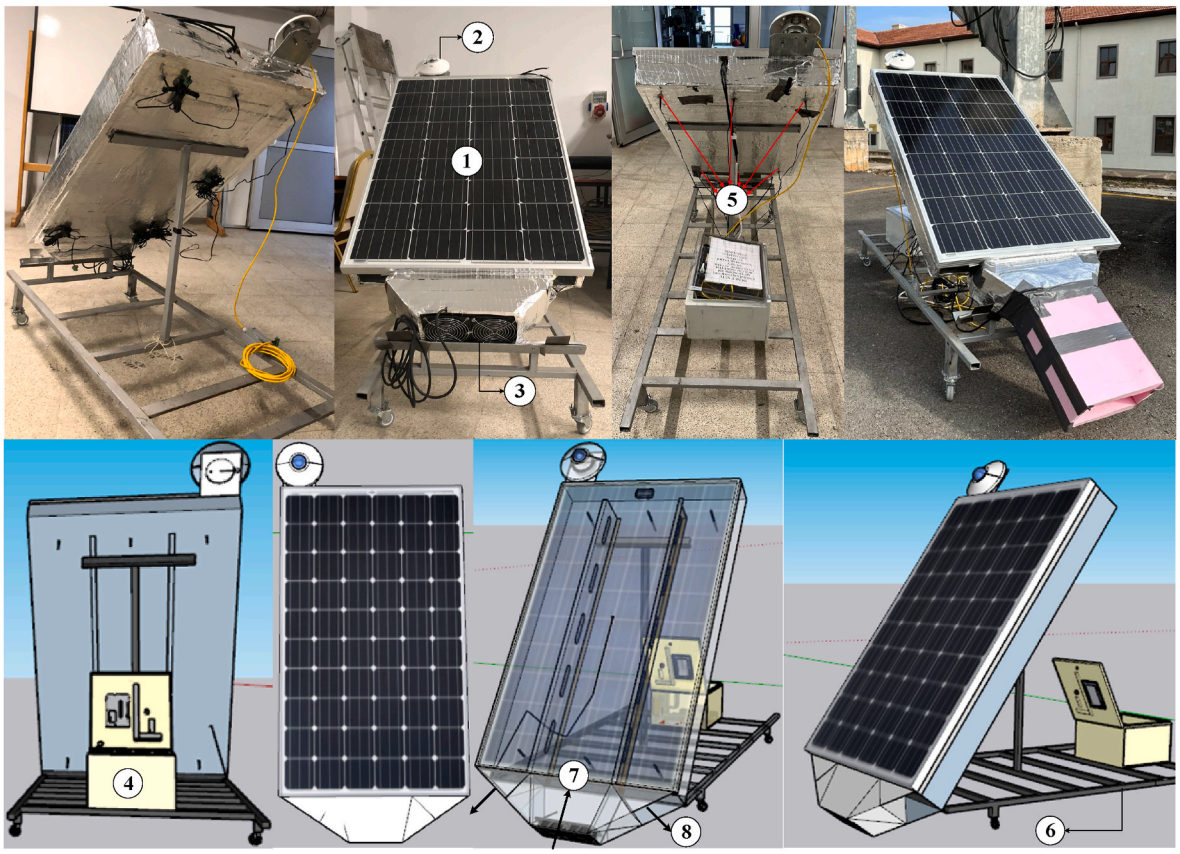


**Fig. 6.** Design and assembly of absorber plate. 1: Monocrystalline PV collector, 2: Pyranometer, 3: Fan group, 4: Data logger and control board, 5: NTC temperature measurements, 6: Platform, 7: Ambient air inlet, 8: Indoor air outlet.

temperature are given in Fig. 5. While the outlet air temperature in perforated PVT was measured as 20.9 °C in the numerical study, this value was measured as 20.4 °C on average in the experimental study. Numerical study was carried out with a 2.4 % error approach.

## 2.2. Experimental set-up

### 2.2.1. Design of the absorber plate

Based on the numerical analysis in Section (3.1), the usage of perforated structure resulted in a 13.2 % enhancement in thermal efficiency and a 0.19 % improvement in electrical efficiency. According to numerical analysis, electrical and thermal efficiencies of the perforated fin collector are higher than those of the unperforated collector. So, the perforated fin structure is applied to PVT system.

Novelty of this study is the absorber plate design. The absorber plate design of the air source PVT was specially manufactured for the system from copper material with a surface area of 0.085 $m^2$. Two pieces of 950 × 100 $mm^2$ dimensions were manufactured and mounted back of the PV system, creating a contact surface area of 0.019 $m^2$, as seen in Fig. 6.

Airflow diagram and temperature measurement points in the PVT design are shown in Figs. 7 and 8. Air tightness was achieved between the absorber plate by closing the back surface of the PVT design. It was installed to allow external air movement into the system through the 300 mm gap between two absorber plates, to the PV rear surface and the absorber plate surface. Fresh air entered from the middle point of the PVT. It was designed to return through the 5 vents created on both absorber plates and the 200 mm gap left at the end point of the absorber plate. The fresh air was discharged to the outside by drawing the heat load from the PVT through the 185 mm gaps on both sides of the inlet point. The air discharge point of the PVT was designed, as shown in Fig. 7, to be directed opposite the air suction point of the fans to avoid loss of efficiency in the PV system.

### 2.2.2. Description of PVT

In this study, the PVT was designed with special copper plates and a monocrystalline structure with 36 cells. A new design model was developed using a PV collector of 1150 × 670 × 30 mm dimension, two fans measuring 120 × 120 mm with 12V output, and a control collector that adjusts the fan speed by recording and processing the data received from the sensors. The equipment used in the PVT and their features are given in Table 2.

### 2.2.3. Design of the control board

A control board and datalogger topology, shown in Fig. 9, were developed to record the data of the PVT and control the cooling fan velocity. This control board and datalogger can measure the voltage, current, and surface temperature of the PV collector, solar irradiation, temperatures in the air tunnel, and ambient relative humidity. The developed board contains a Li-ion battery with a capacity of 22.2 V 10 Ah. This battery provides power supplies for all units in the PVT. Thus, measurements of the PVT system were carried out independently of the grid. Direct current (DC)/DC converter circuits are at terminals of the Li-ion battery output. These DC/DC converter circuits can output different voltages required by the control boards, fans, and sensor converter units. It used 12-bit ADC resolution control cards with two STM32F103C8T6 processors on the control and data logger board. A total of 20 different sensor data can be measured with these two boards. Control boards record the measured data onto secure digital (SD) cards every minute.

Solar irradiation was measured with the Kipp&Zonen brand SMP22 pyranometer model. The current of the PV collector was measured with a LEM brand LA 200-P hall-effect sensor. The negative temperature coefficient (NTC) type is preferred for temperature probes. Temperature

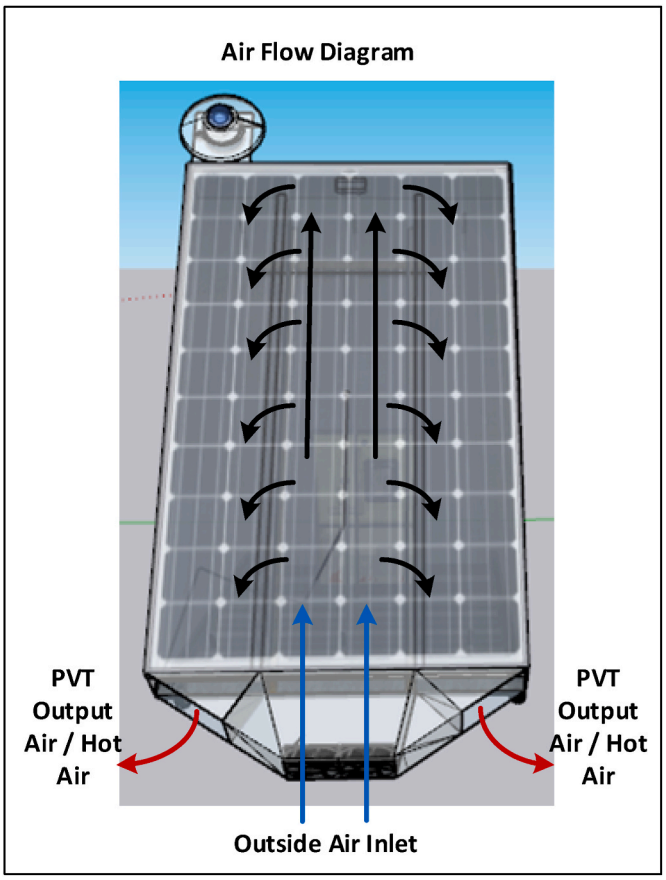


**Fig. 7.** Airflow diagram of PVT system.

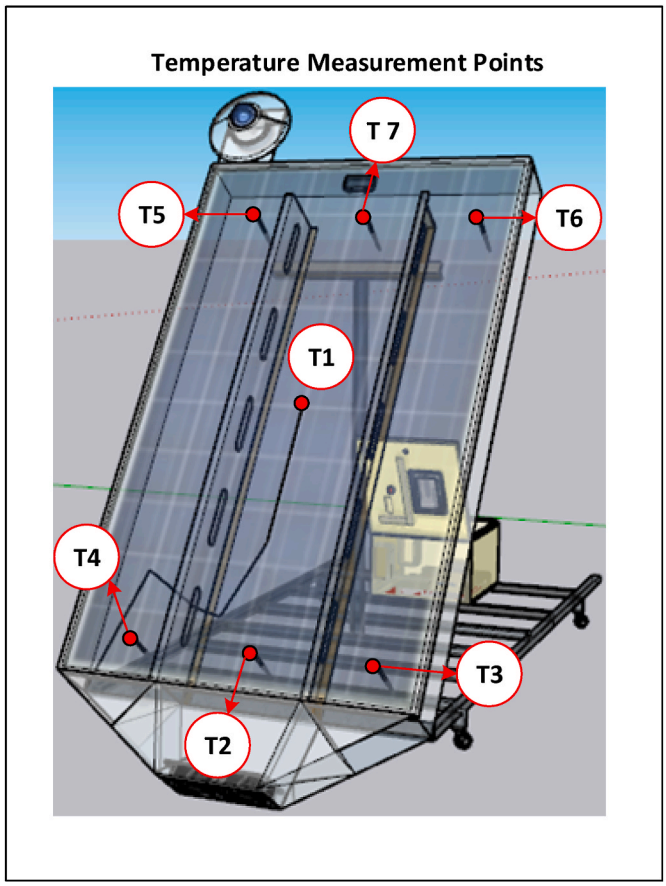


**Fig. 8.** Temperature measurement points of PVT system.

and relative humidity measurements of the environment were carried out using humidity and temperature sensors of the Notion Control brand. Two 12 V 0.6 A brushless fans were used to cool the PVT. All measurements made with the control and datalogger card were confirmed with calibrated measuring devices. Fig. 10 shows the photograph of the control card and datalogger circuit board developed for the PVT.

### 2.2.4. Experimental procedure

This study conducted three consecutive experiments in February 2024 at 39.93° North latitude and 32.86° East longitude. The experiment performed on the first, second, and third days were named Experiment 1, Experiment 2, and Experiment 3, respectively. The experiments started at 10:30 a.m. and continued until 3:30 p.m. Measurements were recorded by the datalogger every minute from the points shown in Fig. 8.

In this study, the temperature of the PV collector is measured with the $T_1$ temperature probe placed on the back surface of the PV. For the PV collector to work efficiently, the temperature of the PV collector is controlled at a temperature of 25 °C. In conventional PVT cooling systems, the surface temperature of the PV collector is cooled by fans with a constant flow rate. Although a low-flow airflow is required for the PV collector, the fan is constantly operated at a steady speed in constant-flow cooling systems. In this case, while a low-power fan is needed for cooling, the cooling process is carried out with excess energy. This study provides cooling at different fan speeds with 5 °C intervals between the PV collector surface temperature from 25 to 40 °C. Thus, cooling is carried out at low fan power in cases of low cooling need, and in cases where high heat is required, cooling is carried out at high fan power. The originality of this study is provided by the temperature controlled with variable air volume for the PV cooling feature. For this purpose, the PVT system's electrical and thermal efficiency was contributed. The fan started working when the temperature value from point $T_1$ exceeded 25 °C. It operated by increasing the fan speed until the temperature reached 40 °C. The PV collector cooling fan is operated at four different speed levels: 1.5 m/s, 2.2 m/s, 2.9 m/s, and 3.6 m/s, with the temperature control algorithm, depending on the surface temperature. The control board shown in Fig. 10 was designed specifically for this PVT, and the measurements were controlled throughout the experiment.

### 2.2.5. Theoretical analysis

Its efficiency can be calculated to analyze the proposed PVT collector's performance. The efficiency of the PVT collector is the sum of electrical ($\eta_{el}$) and thermal ($\eta_{th}$) efficiencies. The overall efficiency of the PVT is below:

$$\eta_{PVT} = \eta_{el} + \eta_{th} \tag{5}$$

The electrical efficiency of the PVT collector can be explained as the ratio of the electrical output power of the PV module ($P_{max}$, W) to the collector area ($A$, $m^2$) and solar irradiance ($S_{irr}$, $W/m^2$). Here, $P_{max}$ is the product of the current ($I_{max}$, A) and voltage ($V_{max}$, V) values measured from the PV module. The electrical efficiency of the PVT collector is given as [31]:

$$\eta_{el} = \frac{P_{max}}{AS_{irr}} = \frac{I_{max}V_{max}}{AS_{irr}} \tag{6}$$

Thermal efficiency is the ratio of useful energy ($\dot{Q}_u, W$) to collector area ($A$, $m^2$) and solar irradiation ($S_{irr}$, $W/m^2$), and thermal efficiency of the PVT can be defined as [32]:

$$\eta_{th} = \frac{\dot{Q}_u}{AS_{irr}} \tag{7}$$

**Table 2**
Features of the equipment used in the PVT system.

| Equipment | Features | | | |
|---|---|---|---|---|
| PVT Collector | Power | Number of the cell | Cell type | Tolerance |
| | 145 W | 36 | Monocrystalline | ±5 % |
| Temperature Sensor | Type | Accuracy | Resistance value at 25 °C | Operating temperature range |
| | NTC | ±0.1 °C | 10 KΩ ±1 % | −30 °C to +105 °C |
| Cooler Fan | Voltage | Current | Dimensions | Speed levels (4) |
| | 12 V | 0.58 A | 12 × 12 × 2 cm | 1.5 m/s, 2.2 m/s, 2.9 m/s, 3.6 m/s |
| Pyranometer | Measurement range | Accuracy | Sensitivity | Nonlinearity (0–1000 W/m$^2$) |
| | 0–2000 W/m$^2$ | < ±5 W/m$^2$ | 5–20 μV/W/m$^2$ | <1 % |
| Thermohygrometer | Temperature range | Temperature accuracy | Relative humidity | Relative humidity accuracy |
| | −20 to 55 °C | ±0.4 °C | 0–100 % | ±2 % |
| PVT back surface cladding/insulated | Cladding material | Insulation material | Area | Thickness |
| | Aluminum sheet | 2.5 m$^2$ | 1.67 m$^2$ | 20 mm |
| Copper Plate | Total area | Dimensions | Thickness | Contact surface area |
| | 0.085 m$^2$ × 2 | 950 × 100 mm × 2 | 2 mm | 0.019 m$^2$ × 2 |

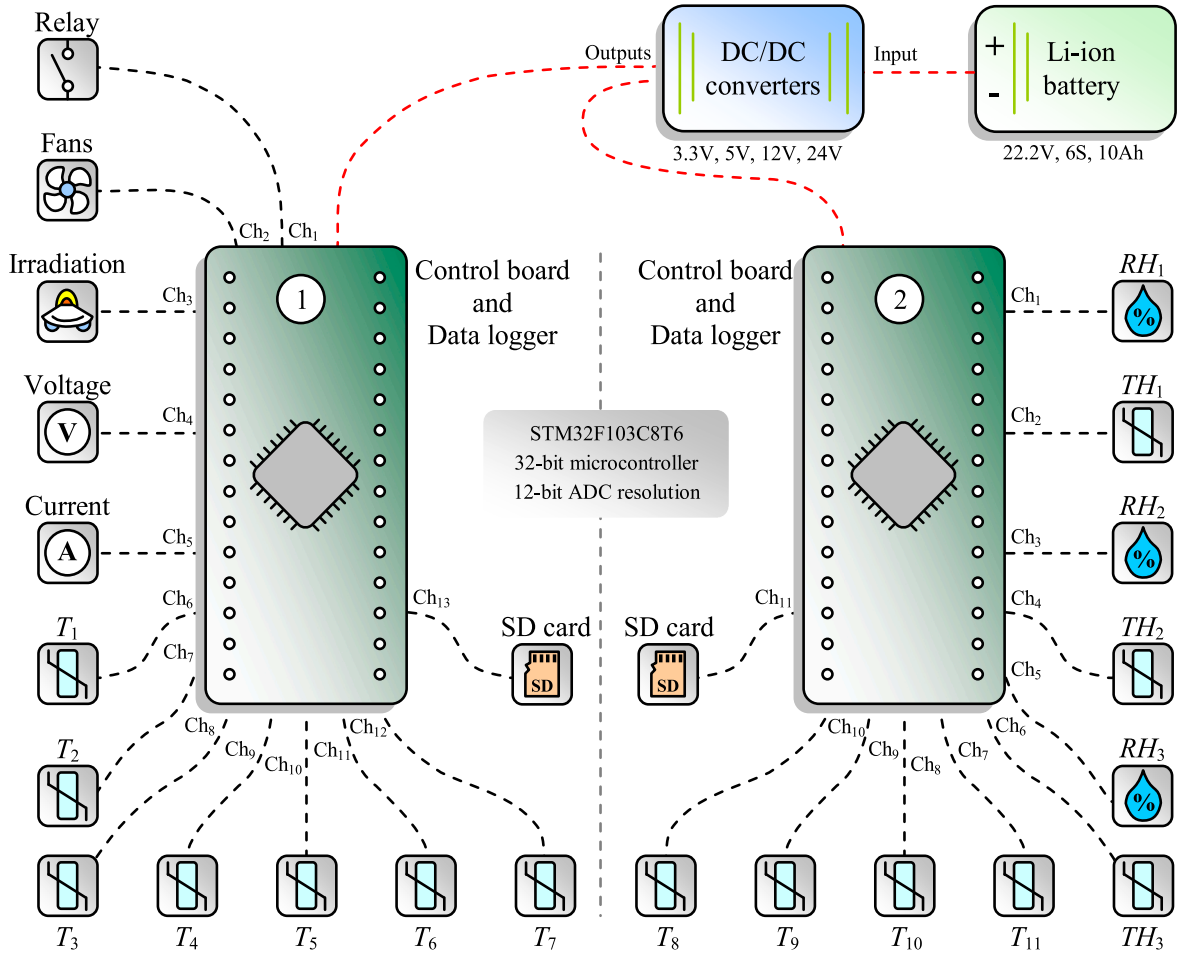


**Fig. 9.** Control board and datalogger circuit topology of the PVT system.

The useful energy here is expressed as follows:

$$\dot{Q}_u = \dot{m}_{air}\, c_{p,air}\, (T_{out}\text{-}T_{in}) \tag{8}$$

In equation (8), $\dot{m}_{air}$ (kg/s), $c_{p,air}$ (J/kgK), $T_{in}$ (K), $T_{out}$ (K) describe the mass flow rate of air, the specific heat of the air, the temperature of the air entering the PVT collector, and the temperature of the air leaving the PVT collector, respectively. The mass flow rate consists of the density of the air ($\rho_{air}$, kg/s), the velocity of the air ($v_{air}$, m/s), and the cross-sectional area ($A_{air}$, m$^2$) through which the air flows and is shown as follows [33]:

$$\dot{m}_{air} = \rho_{air} v_{air} A_{air} \tag{9}$$

The specific heat of air can be calculated by the following formula, where $T_a$ (K) is the ambient temperature [33]:

$$c_{p,air} = 1009.26\text{-}0.0040403T_a + 0.00061759{T_a}^2\text{-}0.0000004097{T_a}^3 \tag{10}$$

The input ($\dot{E}_{x,in}, W$) and output ($\dot{E}_{x,out}, W$) exergy supplied from solar energy can be defined as [33]:

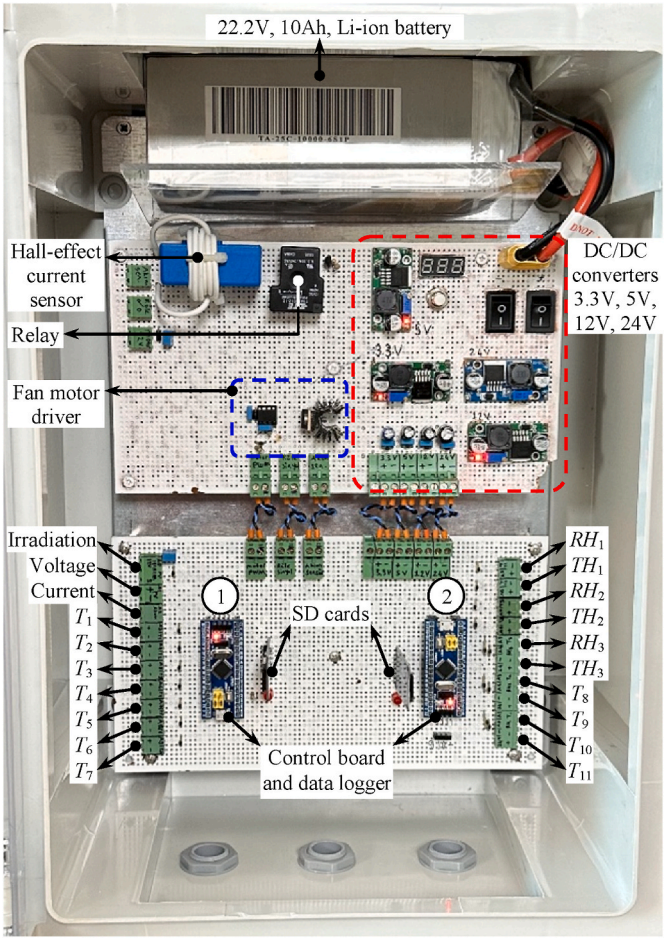


**Fig. 10.** Photograph of the PVT system's control board and datalogger circuit.

$$\dot{E}_{x,in} = AS_{irr}\left[1-\frac{4}{3}\left(\frac{T_a}{T_s}\right)+\frac{1}{3}\left(\frac{T_a}{T_s}\right)^4\right] \tag{11}$$

$$\dot{E}_{x,out=}\ \dot{Q}_{loss}\left(1-\frac{T_a}{T_{\text{cell}}}\right) \tag{12}$$

$T_s$ (K) in Equation (11) is the temperature of the sun (5770 K), $T_{cell}$ (K) in Equation (12) is the cell temperature of the PVT collector, and $\dot{Q}_{loss}$ (W) is the heat loss. Exergy balances are explained in the following equations [33]:

$$\sum \dot{E}_{x,d} = \sum E_{x,in} - \sum E_{x,out} \tag{13}$$

$$\sum \dot{E}_{x,d} = \sum E_{x,in} - \sum \left(E_{x,th} + E_{x,PV}\right) \tag{14}$$

$$\dot{E}_{x,th} = \dot{Q}_u\left(1-\frac{T_a}{T_{out}}\right) \tag{15}$$

$$\dot{E}_{x,PV} = \eta_{el}\, AG\left[1-\frac{4}{3}\left(\frac{T_a}{T_s}\right)+\frac{1}{3}\left(\frac{T_a}{T_s}\right)^4\right] \tag{16}$$

$$\dot{E}_{x,PVT} = E_{x,th} + E_{x,PV} \tag{17}$$

$\dot{E}_{x,d}$ (W) is exergy destruction and the exergy efficiency of the PVT collector [31]:

$$\eta_{ex} = 1-\frac{\dot{E}_{x,d}}{\dot{E}_{in}} = \frac{\dot{E}_{x,out}}{\dot{E}_{x,in}} \tag{18}$$

The annual amount of energy produced by the PVT system was calculated by taking an average of 7.5 h of solar irradiation per day. Electricity and natural gas prices were accepted as 0.07 $/kWh and 0.19 $/m$^3$. In all calculations, the amount spent for the accumulator, charge controller, converter, and other equipment and the entire system is determined as 65 $. The equations were used to calculate the annual amount of electricity produced and the amount that would be consumed if natural gas was used to meet the consumed power.

$$AC_1 = W \times N \times ET \tag{19}$$

$$AC_2 = M_{gas} \times N \times NT \tag{20}$$

In Equations (19) and (20), $W$ is the power consumption, $N$ is the daily working time in a year, and $ET$ and $NT$ are the unit price of electricity and natural gas. The payback period ($PP$) of the PVT system is defined as the ratio between the total investment cost ($TIC$, $) and $AC_{total}$ ($AC_1$ +

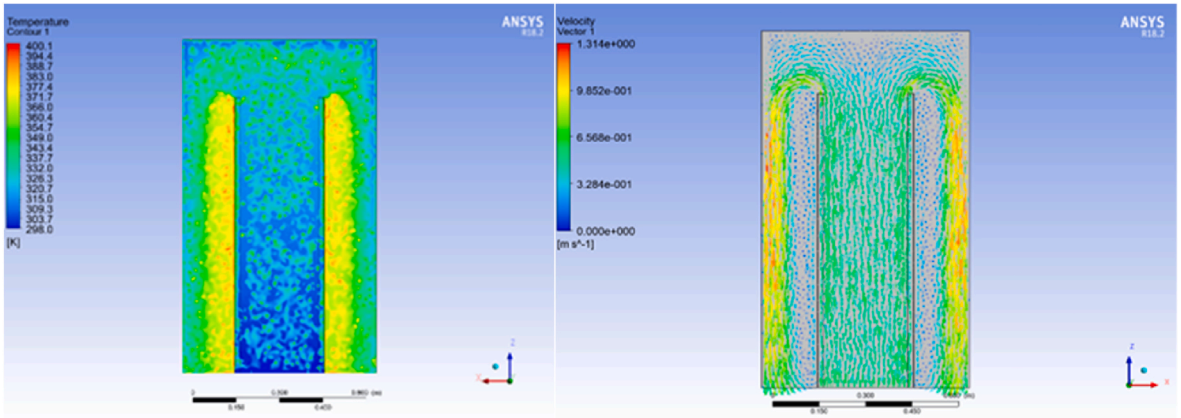


**Fig. 11.** PV surface temperature and velocity distribution of non-perforated collector: a) temperature, b) velocity.

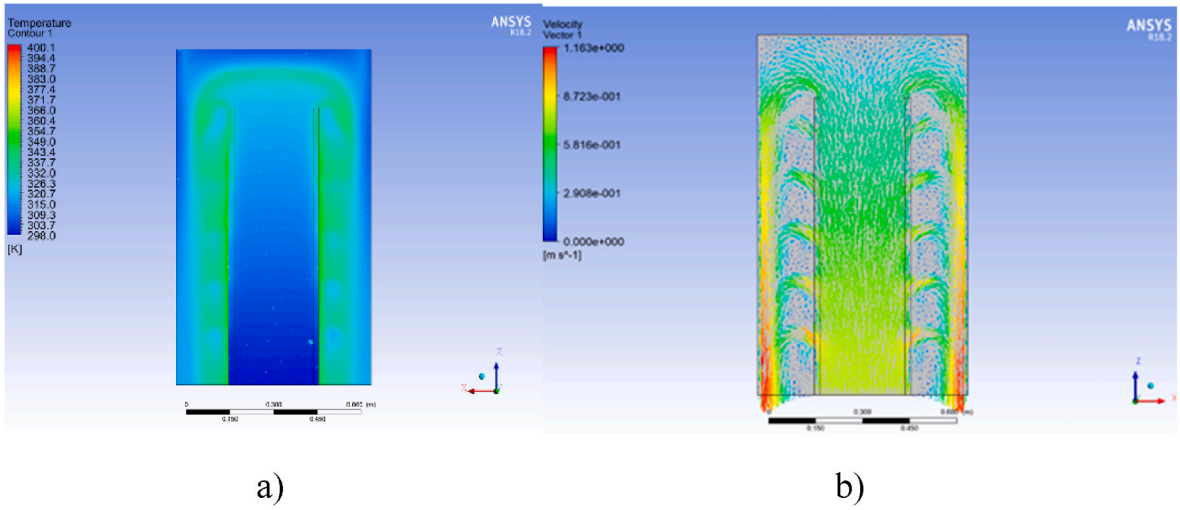


**Fig. 12.** PV surface temperature and velocity distribution of perforated collector: a) temperature, b) velocity.

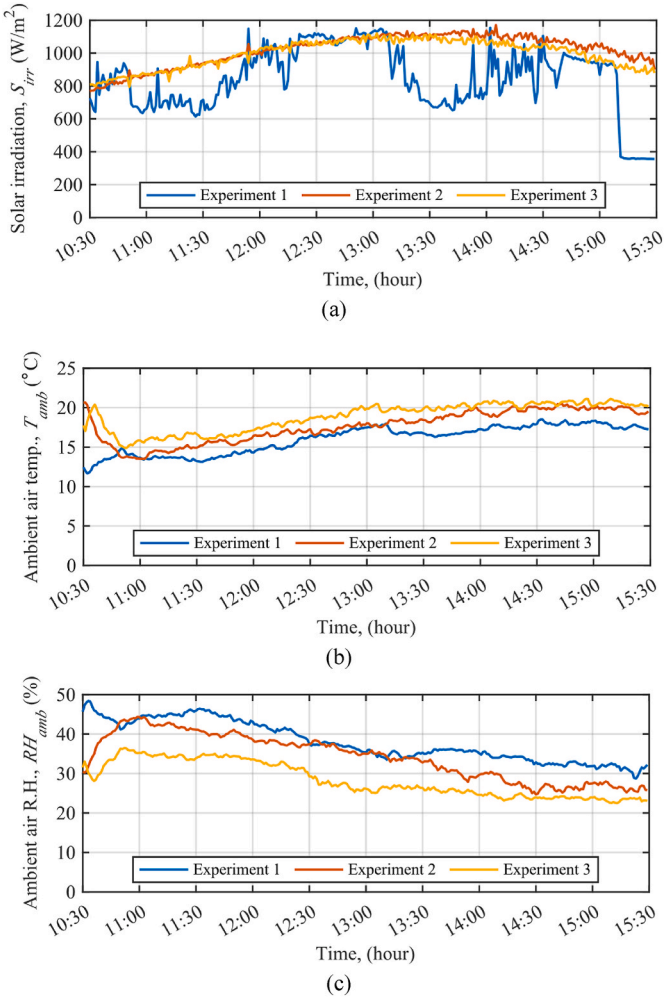


**Fig. 13.** Graphs of the ambient characteristics during three-day experiments, respectively (a) solar irradiation $S_{\text{irr}}$, (b) ambient air temperature $T_{\text{amb}}$, and (c) ambient air relative humidity $RH_{\text{amb}}$.

$AC_2$, $/year) and is expressed as follows [34]:

$$PP = \frac{TIC}{AC_{total}} \tag{21}$$

In experimental studies, the uncertainty arising from measurements or measuring devices must be determined. $R$ is the quantity to be measured, the independent variables affecting the $R$ quantity are expressed as $x_1$, $x_2$, $x_3$, … $x_n$, and the error rates of each independent variable are expressed as $w_1$, $w_2$, $w_3$, … $w_n$. Uncertainty analysis ($W_R$) can be computed with the following equation [35]:

$$W_R = \left[\left(\frac{\delta R}{\partial x_1} w_1\right)^2 + \left(\frac{\delta R}{\partial x_2} w_2\right)^2 + \ldots + \left(\frac{\delta R}{\partial x_n} w_n\right)^2\right]^{1/2} \tag{22}$$

## 3. Results&Discussion

### 3.1. Numerical results

The achieved numerical findings of the PV surface temperature and velocity distribution of non-perforated and perforated collector designs are illustrated in Figs. 11 and 12. While the temperature contours can give a general view of the heating process of flowing air inside the collectors, the velocity contours can show the vortex region created by the airflow. The temperature difference between the temperature of the fluid sent to the PV collector for cooling purposes and the collector surface temperature is at its highest value at the PV air inlet point. As the air flows in the collector, this temperature difference decreases, and heat transfer also decreases. It is known that the PV collector cannot be cooled at points close to the air outlet. For this purpose, in this study, cold air was blown onto the PV collector from the middle point and flowed to the right and left at the top. In addition, air flows from the holes to the right and left from the middle point, and therefore vortexes were formed at the hole exits and the upper right-left points where the turns in this flow occur, which contributed to the increase in heat transfer in the PV collector. These vortexes are in a structure that will eliminate the reduction of dead zones in the PV collector. With the perforation of the fins, the air accumulated in the middle is transferred to the sides. In addition, airflow is provided to the sides of the perforated collector of the velocity vectors. Thus, the large vortex formed on the side of the winglets the gap in Figs. 11 and 12 was prevented. According to the numerical results obtained based on the PV surface temperatures in the collector with perforated and non-perforated fins, results were obtained with an error of 0.05 % and 0.06 %, respectively. As can be seen clearly in temperature and velocity contours, it is seen that a weak

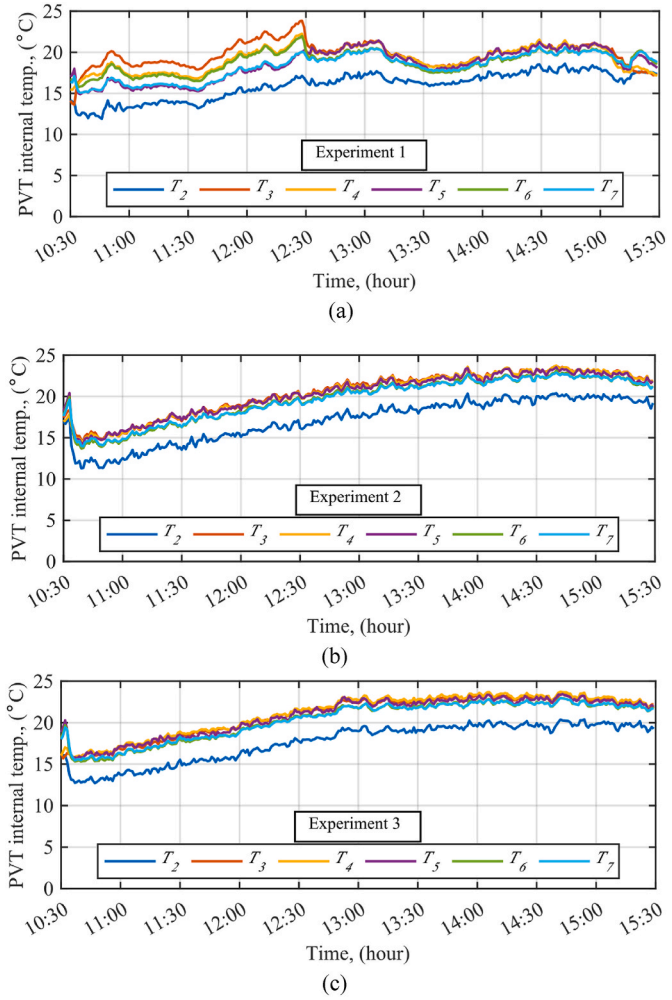


**Fig. 14.** Graphs of changes in the PVT internal temperature points for three different experimental days: (a) Experiment 1, (b) Experiment 2, and (c) Experiment 3, respectively.

**Table 3**
The avarage temperature PVT collector back surface.

| | $T_2$ (°C) | $T_3$ (°C) | $T_4$ (°C) | $T_5$ (°C) | $T_6$ (°C) | $T_7$ (°C) |
|---|---|---|---|---|---|---|
| Experiment 1 | 15.95 | 19.73 | 19.18 | 18.51 | 18.79 | 18.29 |
| Experiment 2 | 17.06 | 20.44 | 20.36 | 20.26 | 19.67 | 19.65 |
| Experiment 3 | 17.63 | 20.9 | 21.12 | 20.82 | 20.31 | 20.32 |

airflow occurs in the non-perforated collector, and a more homogeneous cooling is achieved in the perforated collector.

### 3.2. Experimental results

The experimental examinations were performed over three consecutive days (Experiment 1, Experiment 2, Experiment 3) in February (winter conditions) to test the PVT's electrical and thermal performance. Fig. 13 depicts ambient characteristics and the system's performance, assessed when the PVT showed how the environmental parameters (solar irradiation, ambient air temperature, and relative humidity) change during the day. While solar irradiation values indicated similar values in Experiment 2 and Experiment 3, fluctuations were observed in Experiment 1 due to cloudiness. Solar irradiation values varied between 355.64 and 1154.28 W/m$^2$ in Experiment 1, 767.71 – 1170.46 W/m$^2$ in Experiment 2, and 794.26 – 1120.04 W/m$^2$ in Experiment 3. The average ambient air temperature and relative humidity values were recorded as 16.0 °C, 17.63 °C, 18.83 °C, 38.03 %, 34.19 %, and 28.43 % for three cases, respectively.

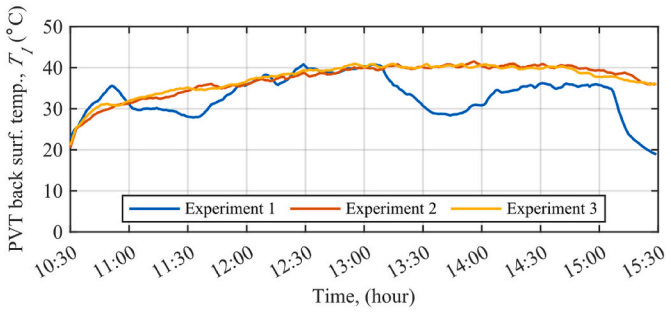


**Fig. 15.** Temperature of the PVT back surface $T_1$ point.

**Table 4**
Boundary conditions for fan speed levels.

| Parameters | Air velocity (m/s) | PVT surface temp. $T_1$ (°C) | Air flow rate (m$^3$/h) |
|---|---|---|---|
| Level 1 | 1.5 m/s | 25 °C–30 °C | 121.0 |
| Level 2 | 2.2 m/s | 30 °C–35 °C | 177.4 |
| Level 3 | 2.9 m/s | 35 °C–40 °C | 230.4 |
| Level 4 | 3.6 m/s | Above 40 °C | 291.6 |

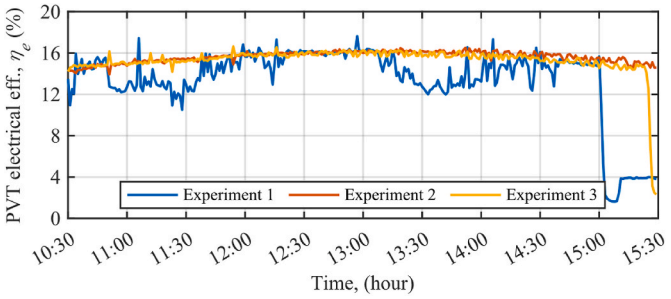


**Fig. 16.** Variation of electrical efficiency values of PVT depending on time.

Fig. 14 illustrates the temperature values measured from the internal temperature points of the PVT. The measurement points of the thermocouples are indicated in Fig. 8. The average temperature values of $T_2$, $T_3$, $T_4$, $T_5$, $T_6$ and $T_7$ were measured and given in Table 3 for Experiment 1, Experiment 2, and Experiment 3. $T_2$ temperature was lower in all three experiments because that is the temperature of fresh air entering the PVT. The instantaneous maximum temperature value was observed as 23.83 °C at $T_3$ temperature at the 120th minute in Experiment 1.

The operation of the fan was adjusted according to the value of the $T_1$ thermocouple on the back surface of the PVT. The fan started to operate when the temperature value of $T_1$ exceeded 25 °C and continued to work until it reached 40 °C. The fan's speed also increased according to the rise in temperature on the PV back surface. The change of $T_1$ temperature throughout the experiment for all three experiments is given in Fig. 15. In Experiment 1, fluctuations in temperature values were also observed depending on the fluctuation in solar irradiation. In the same order, average $T_1$ temperature values were measured as 33.16 °C, 37.14 °C, and 37.3 °C for Experiment 1, Experiment 2, and Experiment 3. Also, the maximum and minimum values are 40.74 °C, 18.87 °C in Experiment 1, 41.54 °C, 20.47 °C in Experiment 2, 40.93 °C, 21.13 °C in Experiment 3. In Experiment 1, after the 280th minute, the $T_1$ temperature value suddenly decreased due to the drop in solar irradiation. With the developed PVT design with a variable air flow rate, the back surface of the PVT could be successfully cooled. In this study, the collector was cooled effectively according to the required temperature ranges without increasing the fan power.

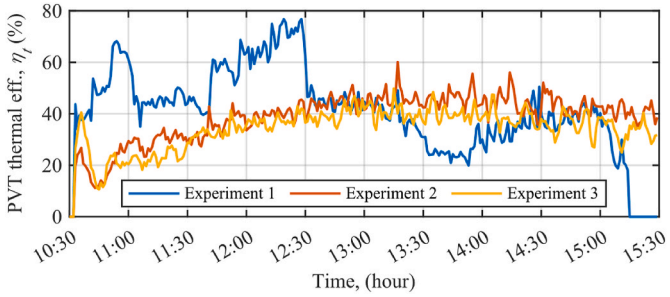


**Fig. 17.** Variation of thermal efficiency values of PVT depending on time.

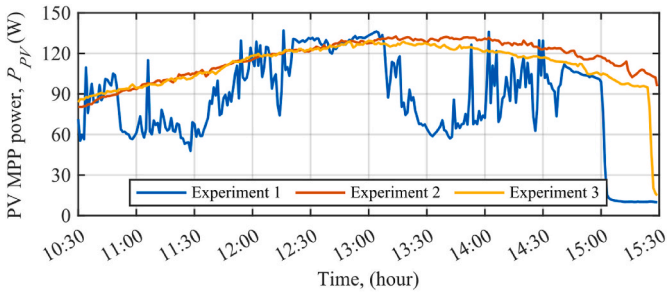


**Fig. 18.** Power change at the PVT collector's maximum power point (MPP) for three experimental days.

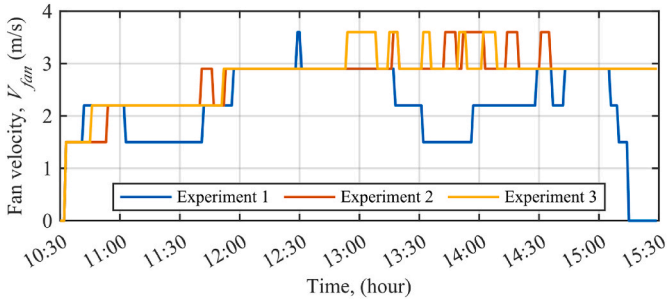


**Fig. 19.** Cooling fan speed change of the PVT system for three experimental days.

Table 4 gives the boundary conditions for fan speed levels. In the experiments, the air flow rate was increased or decreased depending on the PVT back surface temperature. As seen in Fig. 15, the fan flow rate varied according to PVT back surface temperature. Therefore, the temperature changes given in Fig. 14 (a) occurred due to the changing air flow rate in the system. Depending on the amount of solar radiation, the heat flux in the PVT collector and the fan flow rate changed according to the temperature ranges given in Table 4, and temperature fluctuations were observed during the experiments.

The change in electrical efficiency of the cooled collector at different air flow rates is shown in Fig. 16 as a function of time. Electrical efficiency values varied between 1.6 and 17.62 % in Experiment 1, 13.92 – 16.50 % in Experiment 2, and 2.32 – 16.64 % in Experiment 3. Average values were obtained as 13.42 %, 15.63 %, and 15.31 % for three cases, respectively. As seen in Fig. 16, it is seen that the collector generated electrical power without large changes in Experiments 2 and Experiment 3 depending on the variable air flow rate. Fluctuations in the electrical efficiency in Experiment 1 were also observed depending on solar irradiation. According to experimental results, solar irradiance and efficiency had a linear relationship. Electrical efficiency is a function of measured solar irradiance and electrical output power.

Thermal efficiency values obtained from the PVT throughout the experiments are shown in Fig. 17. Thermal efficiency indicates the PVT's thermal performance and is related to solar irradiance, ambient temperature, and relative humidity. The PVT's average thermal efficiency for three cases was calculated as 35.41 %, 28.39 %, and 21.78 %, respectively. The highest thermal efficiency was 76.73 % at the 118th minute in Experiment 1.

The maximum transfer of electrical power produced by the proposed PVT collector to the load can be evaluated with Maximum Power Point (MPP). PVT collector's MPP varies depending on many factors such as solar irradiation, ambient temperature, and solar cell temperature. Fig. 18 depicts the maximum power point of the PVT collector. In Experiment 1, fluctuations are observed depending on solar irradiation. The highest instantaneous PVT collector's MPP was achieved as 136.92 W in Experiment 1. The average PV collector's MPP was obtained as 86.31 W, 116.2 W, and 111.5 W in Experiment 1, Experiment 2, and Experiment 3, respectively.

Fig. 19 demonstrates the cooling fan velocity values of the PVT system during three experiments. The surface temperature of the PVT collector exceeded 25 °C, the fan started to operate. As the temperature rose, the fan velocity increased, providing effective cooling. This study provided the temperature control algorithm with the designed PVT system's control board. According to Fig. 19, the fan velocity varied

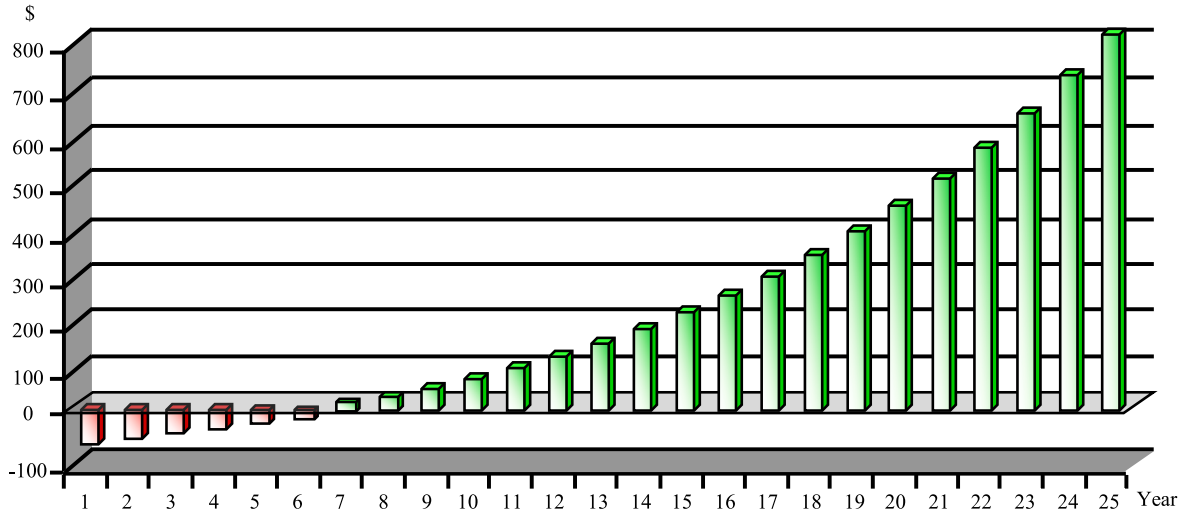


**Fig. 20.** The 25-year depreciation graph of the PVT system.

**Table 5**
Comparison of PVT collectors in this study and the literature.

| Authors | Location | Season | Working fluid | Solar irrad. (W/m$^2$) | Thermal efficiency | Electrical efficiency | Explanation |
|---|---|---|---|---|---|---|---|
| Hazami et al. [40] | Tunisia | Summer | Air | 380–1070 | 50 % | 15 % | Max. exergy of thermal and electrical efficiency 50 % and 14.8 %, respectively. |
| Pang et al. [41] | China | – | Air | 743 | 53.08 % | 13.67 % | Experiments were carried laboratory conditions and generated power of the PVT was increased by cooler circulation. |
| Fterich et al. [42] | Tunisia | Spring | Air | 800 | 42.50 % | – | They noted that increasing cell temperature has an undesirable effect on electrical efficiency. |
| Ahn et al. [43] | South Korea | Winter | Air | 700–1050 | 23 % | 15 % | Efficiency of the PVT with heat recovery was found to be 38 %, while the efficiency of the ventilation with heat recovery increased to 20 % with the preheating air from the PVT. |
| Mojumder et al. [44] | Malaysia | – | Air | 700 | 56 % | 13.75 % | As the mass flow rate increased (0.02–0.14 kg/s) thermal efficiency increased from (37.82–56.19 %). |
| Zabihi Sheshpoli et al. [45] | Iran | Summer | Water | – | 37 % | 14.84 % | They saw that the average total efficiency goes up to 51.76 % when the flow rate is at its highest. |
| Saygın et al. [46] | Türkiye | Summer | Air | 660.6 | 48 % | 7.7 % | There should be 3 cm of space between the glass covering and the collector for the best thermal efficiency. There should be 5 cm of space between them for the best electricity efficiency. |
| Özakın and Kaya [47] | Türkiye | Summer | Air | 950–1000 | 59 % (polycrystal collector) and 48 % (monocrystal collector) | – | To increase heat transfer and provide more efficient cooling, cylindrical aluminum fins have been placed to the air cooling channel. |
| Özakın and Kaya [48] | Türkiye | Summer | Air | – | For the monocrystal collector, sparse and frequent fin configurations are 61.4%–65.4 % and 79%–83.4 % for copper fins, respectively, 57.9%–60.7 % and 64–65.8 % for aluminum fins, 54.5%–57 % and 59–63 % for brass fins respectively. For the polycrystal collector, sparse and frequent fin configurations are 59.7%–63.2 % and 71.4%–75.5 % for copper fins, respectively, 56.2%–58.8 % and 57.5–59 % for aluminum fins, respectively, 52.7%–54.5 % and 50.6–53.5 % for brass fins respectively. | For the monocrystal collector, sparse and frequent fin configurations are 11.87%–12.63 % and 12.91%–13.94 % for copper fins, respectively, 11.32%–11.94 % and 11.96–12.6 % for aluminum fins, respectively, 10.88%–11.02 % and 11.05–11.41 % for brass fins respectively. For the polycrystal collector, sparse and frequent fin configurations are 11.6%–12.35 % and 12.5%–13.47 % for copper fins, respectively, 11.24%–11.85 % and 11.53–12.3 % for aluminum fins, respectively, 10.80%–11 % and 10.87–11.23 % for brass fins respectively. | For the monocrystal collector, it is concluded that the ideal fins number is 55 for copper and aluminum and 27 for brass. For polycrystal penel, both thermal and exergy efficiencies for frequent configuration brass fins were lower than those for sparse configuration. |
| Alfegi et al. [49] | Malaysia | – | Air | 400 | 17%–26.43 % | 10.50%–12.09 % | Compound parabolic collector and fins have a potential to significantly increase in power production and reduce the cost of photovoltaic electricity. |
| Priyam and Chand [50] | India | Spring | Air | 858.3–872.29 | 70 % | – | It is concluded that the wavy fin solar air heater with the lowest fin spacing (2 cm) performs better than higher fin spacing (6 cm) due to the enhanced heat transfer area by narrowing the channel. |

(*continued on next page*)

**Table 5** (*continued*)

| Authors | Location | Season | Working fluid | Solar irrad. (W/m$^2$) | Thermal efficiency | Electrical efficiency | Explanation |
|---|---|---|---|---|---|---|---|
| Chand et al. [51] | India | Winter | Air | 565.66–866.37 | 70 % | – | The results indicate that thermal efficiency increased with increasing flow rate, thermal efficiency, and outlet temperature obtained a maximum of 70 % and 58.66 °C, respectively, for spacing of 2 cm. |
| Chabane et al. [52] | Algeria | | Air | For a flat-plate; 895–900 for solar collector with fins; 753-755 | With fins 40.02%–51.50 %, without fins34.92-to 43.94 % | – | The highest collector efficiency and air temperature rise were achieved by the finned collector with a tilt angle of 45°. In contrast, the collector obtained the lowest values without fins. |
| This study | Türkiye | Winter | Air | Exp.1: 355.64–1154.28 Exp. 2: 767.71–1170.46 Exp. 3: 794.26–1120.04 | Exp.1: 43.68 % Exp. 2: 38.98 % Exp. 3: 34.52 % | Exp.1: 13.42 % Exp. 2: 15.63 % Exp.3: 15.32 % | The highest thermal efficiency was realized in Experiment 1 and the highest electrical efficiency in Experiment 2, depending on the experiments performed under different days and conditions and the air volume varying according to the PVT surface temperature. The system's electrical efficiency was kept constant with very low percentage differences throughout the experiments. |

between 0 and 3.6 m/s in Experiment 1, Experiment 2, and Experiment 3. In the experiments, it was seen that successful control was achieved by saving fan power with variable air volume management compared to the constant airflow system. In Experiment 1, it was seen that the fan velocity decreased when solar irradiation was low because the low solar intensity caused a decrease in the PVT collector surface temperature.

In addition, the uncertainty values were calculated as ±1.04 % for solar irradiation, ±2.3 % ambient relative humidity, ±0.43 °C temperature, and ±0.14 °C for ambient temperature measurements.

The 25-year depreciation graph of the PVT system in this study is given in Fig. 20. The payback period was calculated by taking the average of the electricity and heat power obtained for all three experiments. As can be seen from Fig. 20, the payback period of the proposed PVT system was 6 years. It is seen that the system has become exponentially profitable since the 6th year. Consequently, this PVT system has achieved an efficient and sustainable eco-design.

According to the numerical findings, perforated copper plates showed good results regarding heat dissipation in the PVT. $T_1$ temperature was found to be 33.2 °C in the experimental study and 32.9 °C in the numerical study. The difference is calculated as 0.911 %, which is an acceptable level and shows that the results of the experimental study and the numerical study are compatible. For this reason, it was manufactured and tested with a perforated copper plate. The experimental results of this design tested in winter conditions are compared with the results of another research in Table 5. Various studies on the cooling of PVTs in the literature are presented in Table 5 and in addition to these studies, the experimental results of the realized design are also added to table. A successful design was performed when the results were compared with those of other studies.

$T_1$ temperature was found to be 33.2 in the experimental study and 32.9 in the numerical study. The difference is calculated as 0.911 %, which is an acceptable level and shows that the results of the experimental study and the numerical study are compatible.As a result of the exergy calculations, the average exergy efficiency of the PVT system was calculated as 28.02 % for Experiment 1, 30.67 % for Experiment 2, and 30.61 % for Experiment 3. The total average exergy efficiency was calculated as 29.77 %. When the studies were examined, Ahmadinejad and Moosavi [36] determined the exergy efficiency as 19.65–29.82 %, Ünal et al. [37] 27.40 %, Ishak et al. [38] 12.64 % and Tirupati Rao et al. [39] 21.15 %. Accordingly, the exergy efficiencies of the studies are consistent with the literature.

In the literature, the studies on this subject were conducted with constant air volume and there needs to be more literature on using variable air volume. The gap in the literature is filled in this study where temperature-dependent variable air volume is used. By using variable air volume, efficiency is achieved compared to the system with a constant air flow rate, and the thermal energy produced increases as the PVT collector heats up. The increase in temperature with solar irradiation leads to a decrease in the PVT collector's efficiency. With temperature-controlled variable air volume for cooling the PV, the PVT collector is cooled without excess air, and no air is sent if the PVT collector is cold. In this way, in addition to generating thermal energy and electrical energy, carbon emissions emitted to the atmosphere are also reduced. This study presented a structure that will simplify the use of buildings. This design meets the criteria of net positive carbon, ecological footprint, and green manufacturing, which are required in an eco-design due to reducing carbon emissions.

## 4. Conclusion

A new PVT consisting of two perforated copper plates was designed and tested within the research context. With 5 vents on the perforated copper plates, fresh air was successfully distributed homogeneously inside the PVT. In addition, with the control panel designed for this system, the fan's speed changed according to the temperature, and the measurements were recorded every minute. The key numerical and experimental findings can be summarized as follows.

- According to numerical results, the difference between the numerical study and the experimental study is calculated as 0.911 %. This is an acceptable level and shows that the results of the numerical study and the experimental study are in compatible.
- As a result of experimental findings, the PVT internal temperature value achieved a maximum of 23.83 °C in winter.

- It was observed that the average electrical and thermal efficiency of PVT varied between 13.42 % - 15.63 % and 34.52 %–43.68 %. Moreover, the average exergy efficiency of the PVT was obtained as 29.77 %.
- In the proposed PVT system, the maximum MPP was obtained as 136.92 W.
- The system's payback period was calculated as 6.1 years. Consequently, a significant profit can be achieved in 25 years.

The proposed PVT system, which can be integrated into buildings, will support meeting heat and electrical energy. It is a system design recommended for using renewable energy technology in buildings, especially when green manufacturing is considered. This study presents an eco-design with a PVT design that can benefit from solar energy to the maximum efficiency even in winter conditions.

## CRediT authorship contribution statement

**Ahmet Aktaş:** Writing – review & editing, Writing – original draft, Software, Methodology, Investigation. **Meltem Koşan:** Writing – review & editing, Writing – original draft, Methodology, Investigation. **Burak Aktekeli:** Writing – review & editing, Writing – original draft, Methodology, Investigation. **Yaren Güven:** Writing – review & editing, Writing – original draft, Methodology, Investigation. **Erhan Arslan:** Writing – review & editing, Writing – original draft, Methodology, Investigation. **Mustafa Aktaş:** Writing – review & editing, Writing – original draft, Project administration, Methodology, Investigation.

## Declaration of competing interest

The authors declare that they have no known competing financial interests or personal relationships that could have appeared to influence the work reported in this paper.

## Data availability

No data was used for the research described in the article.

## References


[1] Das D, Kalita P, Roy O. Flat plate hybrid photovoltaic-thermal (PVT) system: a review on design and development. Renew Sustain Energy Rev 2018;84:111–30.
[2] Notton G, Motte F, Cristofari C, Canaletti JL. Performances and numerical optimization of a novel thermal solar collector for residential building. Renew Sustain Energy Rev 2014;33:60–73.
[3] Chow TT. A review on photovoltaic/thermal hybrid solar technology. Appl Energy 2010;87(2):365–79.
[4] Almoatham S, Chiasson A, Mulford R, Moreno-Pena M. Development of experimentally validated models for nocturnal cooling of thermal systems with photovoltaic thermal (PVT) modules. Sol Energy 2024;268:112279.
[5] Jia Y, Alva G, Fang G. Development and applications of photovoltaic–thermal systems: a review. Renew Sustain Energy Rev 2019;102:249–65.
[6] Can ÖF, Arslan E, Koşan M, Demirtaş M, Aktaş M, Aktekeli B. Experimental and numerical assessment of PV-TvsPV by using waste aluminum as an industrial symbiosis product. Sol Energy 2022;234:338–47.
[7] Fudholi A, Zohri M, Rukman NSB, Nazri NS, Mustapha M, Yen CH, et al. Exergy and sustainability index of photovoltaic thermal (PVT) air collector: a theoretical and experimental study. Renew Sustain Energy Rev 2019;100:44–51.
[8] Tonui JK, Tripanagnostopoulos Y. Air-cooled PV/T solar collectors with low cost performance improvements. Sol Energy 2007;81:498–511.
[9] Hamada A, Emam M, Refaey HA, Moawed M, Abdelrahman MA. Investigating the performance of a water-based PVT using encapsulated PCM balls: an experimental study. Energy 2023;284:128574.
[10] Fudholi A, Sopian K, Yazdi MH, Ruslan MH, Ibrahim A, Kazem HA. Performance analysis of photovoltaic thermal (PVT) water collectors. Energy Convers Manag 2014;78:641–51.
[11] Koşan M, Demirtaş M, Aktaş M, Dişli E. Performance analyses of sustainable PVT assisted heat pump drying system. Sol Energy 2020;199:657–72.
[12] Kumar A, Baredar P, Qureshi U. Historical and recent development of photovoltaic thermal (PVT) technologies. Renew Sustain Energy Rev 2015;42:1428–36.
[13] Nkurikiyimfura I, Wang Y, Safari B, Nshingabigwi E. Electrical and thermal performances of photovoltaic/thermal systems with magnetic nanofluids: a review. Particuology 2021;54:181–200.
[14] Dolgun GK, Koşan M, Kayfeci M, Georgiev AG, Keçebaş A. Life cycle assessment and cumulative energy demand analyses of a photovoltaic/thermal system with MWCNT/Water and GNP/Water nanofluids. Processes 2023;11(3):832.
[15] Liu L, Shalwan A, Teng J, Liu C, Li Z. The entropy generation analysis of a PVT solar collector with internally needle finned serpentine absorber tube. Eng Anal Bound Elem 2023;155:1123–30.
[16] Tripty TA, Nasrin R. Efficiency upgrading of solar PVT finned hybrid system in Bangladesh: flow rate and temperature influences. Heliyon 2024;10(7):28323.
[17] Arslan E, Aktaş M, Can ÖF. Experimental and numerical investigation of a novel photovoltaic thermal (PVT) collector with the energy and exergy analysis. J Clean Prod 2020;276:123255.
[18] Abuşka M, Şevik S. Energy, exergy, economic and environmental (4E) analyses of flat-plate and V-groove solar air collectors based on aluminium and copper. Sol Energy 2017;158:259–77.
[19] Yu Q, Chan S, Chen K, Zhao B, Ren X, Pei G. Numerical and experimental study of a novel vacuum photovoltaic/thermal (PVT) collector for efficient solar energy harvesting. Appl Therm Eng 2024;236:121580.
[20] Guo C, Ji J, Sun W, Ma J, He W, Wang Y. Numerical simulation and experimental validation of tri-functional photovoltaic/thermal solar collector. Energy 2015;87:470–80.
[21] Kumar R, Rosen MA. Performance evaluation of a double pass PVT solar air heater with and without fins. Appl Therm Eng 2011;31:1402–10.
[22] Maurya OK, Ekka JP, Kumar D, Dewangan D, Singh A. Experimental and numerical methods for the performance analysis of a tubular three-pass solar air heater. Energy 2023;283:128640.
[23] Joo HJ, An YS, Kim MH, Kong M. Long-term performance evaluation of liquid-based photovoltaic thermal (PVT) modules with overheating-prevention technique. Energy Convers Manag 2023;296:117682.
[24] Hamada A, Emam M, Refaey HA, Moawed M, Abdelrahman MA, Elsayed MEA. Identification of a different design of a photovoltaic thermal collector based on fuzzy logic control and the ARMAX model. Therm Sci Eng Prog 2024;48:102395.
[25] Emam M, Hamada A, Refaey HA, Moawed M, Abdelrahman MA, Rashed MR. Year-round experimental analysis of a water-based PVT-PCM hybrid system: comprehensive 4E assessments. Renew Energy 2024;226:20354.
[26] Zareie Z, Ahmadi R, Asadi M. A comprehensive numerical investigation of a branch-inspired channel in roll-bond type PVT system using design of experiments approach. Energy 2024;286:129452.
[27] Arslan E, Can ÖF, Koşan M, Demirtaş M, Aktekeli B, Aktaş M. Numerical and experimental assessment of a photovoltaic thermal collector using variable air volume. Therm Sci Eng Prog 2023;39:101735.
[28] Khelifa A, Attia MH, Driss Z, Manokar AM. Performance enhancement of photovoltaic solar collector using fins and bi-fluid: thermal efficiency study. Sol Energy 2023;263:111987.
[29] Cfx-Solver A. Theory guide. Release ll. 2006.
[30] https://gepa.enerji.gov.tr/MyCalculator/pages/6.aspx. [Accessed 2 April 2024].
[31] Sardarabadi M, Hosseinzadeh M, Kazemian A, Passandideh-Fard M. Experimental investigation of the effects of using metal-oxides/water nanofluids on a photovoltaic thermal system (PVT) from energy and exergy viewpoints. Energy 2017;138:682–95.
[32] Zare D, Minaei S, Mohamad ZM, Khoshtaghaza MH. Computer simulation of rough rice drying in a batch dryer. Energy Convers Manag 2006;47:3241–54.
[33] Nazri NS, Fudholi A, Mustafa W, Yen CH, Mohammad M, Ruslan MH, Sopian K. Exergy and improvement potential of hybrid photovoltaic thermal/thermoelectric (PVT/TE) air collector. Renew Sustain Energy Rev 2019;111:132–44.
[34] Li X, Zhang Y, Fang L, Jin Z, Zhang Y, Yu X, Ma X, Deng N, Wu Z. Energy, exergy, economic, and environmental analysis of an integrated system of high-temperature heat pump and gas separation unit. Energy Convers Manag 2019;198:111911.
[35] Abdul-Ganiyu S, Quansah DA, Ramde EW, Seidu R, Adaramola MS. Techno-economic analysis of solar photovoltaic (PV) and solar photovoltaic thermal (PVT) systems using exergy analysis. Sustain Energy Technol Assessments 2021;47:101520.
[36] Ahmadinejad M, Moosavi R. Energy and exergy evaluation of a baffled-nanofluid-based photovoltaic thermal system (PVT). Int J Heat Mass Tran 2023;203:123775.
[37] Ünal F, Temir G, Köten H. Energy, exergy and exergoeconomic analysis of solar-assisted vertical ground source heat pump system for heating season. J Mech Sci Technol 2018;32:3929–42.
[38] Ishak MAAB, Ibrahim A, Fazlizan A, Fauzan MF, Sopian K, Rahmat AA. Exergy performance of a reversed circular flow jet impingement bifacial photovoltaic thermal (PVT) solar collector. Case Stud Therm Eng 2023;49:103322.
[39] Tirupati Rao V, Yendaluru RS, Arıcı M, Pochont NR, Reddy Prasad DM. Experimental investigations on bi-symmetrical web flow water based photovoltaic-thermal (PVT) system: energy, exergy, and entropy (3-E) analysis. Sol Energy 2024;271:112445.
[40] Hazami M, Riahi A, Mehdaoui F, Nouicer O, Farhat A. Energetic and exergetic performances analysis of a PVT (photovoltaic thermal) solar system tested and simulated under to Tunisian (North Africa) climatic conditions. Energy 2016;107:78–94.
[41] Pang W, Zhang Q, Wilson GJ, Yang Q, Yan H. Empirical influence of various environmental conditions and mass flow rates on hybrid photovoltaic thermal modules. Appl Therm Eng 2020;171:114965.
[42] Fterich M, Chouikhi H, Sandoval-Torres S, Bentaher H, Elloumi A, Maalej A. Numerical simulation and experimental characterization of the heat transfer in a PVT air collector prototype. Case Stud Therm Eng 2021;27:101209.
[43] Ahn JG, Kim JH, Kim JT. A study on experimental performance of air-type PVT collector with HRV. Energy Proc 2015;78:3007–12.

[44] Mojumder JC, Chong WT, Ong HC, Leong KY, Al-Mamoon Abdullah. An experimental investigation on performance analysis of air type photovoltaic thermal collector system integrated with cooling fins design. Energy Build 2016; 130:272–85.
[45] Zabihi A, Jahanian O, Nikzadfar K, Delavar M. Numerical and experimental investigation on the performance of hybrid PVThermal systems in the north of Iran. Sol Energy 2021;215:108–20.
[46] Saygın H, Nowzari R, Mirzaei N, Aldabbagh LBY. Performance evaluation of a modified PVT solar collector: a case study in design and analysis of experiment. Sol Energy 2017;141:210–21.
[47] Özakın AN, Kaya F. Effect on the exergy of the PVT system of fins added to an air-cooled channel: a study on temperature and air velocity with ANSYS Fluent. Sol Energy 2019;185:561–9.
[48] Özakın AN, Kaya F. Experimental thermodynamic analysis of air-based PVT system using fins in different materials: optimization of control parameters by Taguchi method and ANOVA. Sol Energy 2020;197:199–211.
[49] Alfegi MEA, Sopian K, Othman MYH, Yatim BB. Experimental investigation of single pass, double duct photovoltaic thermal (PV/T) air collector with CPC and fins. Am J Appl Sci 2008;5(7):866–71.
[50] Priyam CP. Experimental investigations on thermal performance of solar air heater with wavy fin absorbers. Heat Mass Tran 2019;55:2651–66.
[51] Chand S, Chand P, Kumar GH. Thermal performance enhancement of solar air heater using louvered fins collector. Sol Energy 2022;239:10–24.
[52] Chabane F, Moummi N, Benramache S. Experimental study of heat transfer and thermal performance with longitudinal fins of solar air heater. J Adv Res 2014;5 (2):183–92.